

ICES REPORT 10-25

June 2010

A New Discontinuous Petrov-Galerkin Method with Optimal Test Functions. Part V: Solution of 1d Burgers' and Navier-Stokes Equations

by

J. Chan, L. Demkowicz, R. Moser, N. Roberts



The Institute for Computational Engineering and Sciences
The University of Texas at Austin
Austin, Texas 78712

Reference: J. Chan, L. Demkowicz, R. Moser, N. Roberts, "A New Discontinuous Petrov-Galerkin Method with Optimal Test Functions. Part V: Solution of 1d Burgers' and Navier-Stokes Equations", ICES REPORT 10-25, The Institute for Computational Engineering and Sciences, The University of Texas at Austin, June 2010.

A NEW DISCONTINUOUS PETROV-GALERKIN METHOD WITH OPTIMAL TEST FUNCTIONS

Part V: SOLUTION OF 1D BURGERS' AND NAVIER-STOKES EQUATIONS

J. Chan, L. Demkowicz, R. Moser, N. Roberts

Institute for Computational Engineering and Sciences
The University of Texas at Austin, Austin, TX 78712, USA

Abstract

We extend the *hp* Petrov-Galerkin method with optimal test functions of Demkowicz and Gopalakrishnan to nonlinear 1D Burgers' and compressible Navier-Stokes equations. With a fully resolved shock structure, we are able to solve problems with Reynolds number up to $Re = 10^{10}$ with double precision arithmetic.

Key words: compressible Navier-Stokes equations, *hp*-adaptivity, Discontinuous Petrov Galerkin

AMS subject classification: 65N30, 35L15

Acknowledgment

The research was supported in by the Department of Energy [National Nuclear Security Administration] under Award Number [DE-FC52-08NA28615]. Demkowicz was also partly supported by a research contract with Boeing. We would like to thank David Young at Boeing for his constant encouragement and support.

1 Introduction

For the past half-century, problems in computational fluid dynamics (CFD) have been solved using a multitude of methods, many of which are physically motivated, and thus applicable only to a small number of problems and geometries. We consider more general methods, whose framework is applicable to different problems in CFD; however, our specific focus will be on the nonlinear shock problems of compressible aerodynamics. Broadly speaking, the most popular general methods include (in historical order) finite difference methods, finite volume methods, and finite element methods.

For linear problems, finite difference (FD) methods approximate derivatives based on interpolation of pointwise values of a function. FD methods were popularized first by Lax, who introduced the concepts of the monotone scheme and numerical flux. For the conservation laws governing compressible aerodynamics,

FD methods approximated the conservation law, using some numerical flux to reconstruct approximations to the derivative at a point. Finite volume (FV) methods are similar to finite difference methods, but approximate the integral version of a conservation law as opposed to the differential form. FD and FV have roughly the same computational cost/complexity; however, the advantage of FV methods over FD is that FV methods can be used on a much larger class of discretizations than FD methods, which require uniform or smooth meshes.

For nonlinear shock problems, the solution often exhibits sharp gradients or discontinuities, around which the solution would develop spurious Gibbs-type oscillations. Several ideas were introduced to deal with oscillations in the solution near a sharp gradient or shock: artificial viscosity parameters, total variation diminishing (TVD) schemes, and slope limiters. However, each had their drawbacks, either in terms of loss of accuracy, dimensional limitations, or problem-specific parameters to be tuned [24]. Harten, Enquist, Osher and Chakravarthy introduced the essentially non-oscillatory (ENO) scheme in 1987 [17], which was improved upon with the weighted essentially non-oscillatory (WENO) scheme in [19]. WENO remains a popular choice today for both finite volume and finite difference schemes.

Well-adapted to elliptic and parabolic PDEs, finite element methods (FEM) gained early acceptance in engineering mechanics problems, though FEM became popular for the hyperbolic problems of CFD later than FD and FV methods. Early pioneers of the finite element method for CFD included Zienkiewicz, Oden, Karniadakis, Hughes [10]. Of special note is the Streamline Upwind Petrov-Galerkin method (SUPG) of Brooks and Hughes [6], which biases the standard test function by some amount in the direction of convection. SUPG is still the most popular FEM stabilization method to date.

Discontinuous Galerkin (DG) methods form a subclass of FEM; first introduced by Reed and Hill in [22], these methods were later analyzed by Cockburn and Shu [11] and have rapidly gained popularity for CFD problems. Rather than having a continuous basis where the basis function support spans several element cells, DG opts instead for a discontinuous, piecewise polynomial basis, where, like FV schemes, a numerical flux facilitates communication between discontinuities (unlike FV methods, however, there is no need for a reconstruction step). Advantages include easily modified local orders of approximation, easy adaptivity in both h and p , and efficient parallelizability. Additionally, DG can handle complicated mesh geometries and boundary conditions more readily than FV or FD methods, and boasts a stronger provable stability than other methods. However, to maintain this stability in the presence of discontinuities/sharp gradients would require additional user-tuned stabilizations, such as artificial viscosity or flux/slope limiters [9].

The Discontinuous Petrov-Galerkin method introduced by Demkowicz and Gopalakrishnan in [13, 14, 15] (DPG), falls under the DG category, but avoids the restrictions and stabilizing parameters of the previous methods. Inherent in the DPG is not only the flexibility of DG, but a stronger proven stability (in fact, optimality) without extra stabilizing parameters, even in the presence of sharp gradients or discontinuities.

2 Discontinuous Petrov Galerkin Method

The concept and name of the *Discontinuous Petrov Galerkin* (DPG) method were introduced by Bottasso, Micheletti, Sacco and Causin in [4, 5, 7, 8]. The critical idea of optimal test functions computed on the fly was introduced by Demkowicz and Gopalakrishnan in [13, 14, 15].

In the following paragraphs, we recall the main ideas of the Petrov–Galerkin method with optimal test functions, and discuss a generalization of it to non-linear problems.

2.1 Petrov-Galerkin Method with Optimal Test Functions

Variational problem and energy norm. Consider an arbitrary abstract variational problem,

$$\begin{cases} u \in U \\ b(u, v) = l(v), \quad \forall v \in V \end{cases} \quad (2.1)$$

Here U, V are two real Hilbert spaces and $b(u, v)$ is a continuous bilinear form on $U \times V$,

$$|b(u, v)| \leq M \|u\|_U \|v\|_V \quad (2.2)$$

that satisfies the inf-sup condition

$$\inf_{\|u\|_U=1} \sup_{\|v\|_V=1} |b(u, v)| =: \gamma > 0 \quad (2.3)$$

A continuous linear functional $l \in V'$ represents the load. If the null space of the adjoint operator,

$$V_0 := \{v \in V : b(u, v) = 0 \quad \forall u \in U\} \quad (2.4)$$

is non-trivial, the functional l is assumed to satisfy the compatibility condition:

$$l(v) = 0 \quad \forall v \in V_0 \quad (2.5)$$

By the Banach Closed-Range Theorem (see e.g. [21], pp.435,518), problem (2.1) possesses a unique solution u that depends continuously upon the data – functional l . More precisely,

$$\|u\|_U \leq \frac{M}{\gamma} \|l\|_{V'} \quad (2.6)$$

If we define an alternative *energy (residual) norm* equivalent to the original norm on U ,

$$\|u\|_E := \sup_{\|v\|=1} |b(u, v)| \quad (2.7)$$

both the continuity and the inf-sup constant become equal to one. Recalling that the Riesz operator,

$$R : V \ni v \rightarrow (v, \cdot) \in V' \quad (2.8)$$

is an isometry from V into its dual V' , we may characterize the energy norm in an equivalent way as

$$\|u\|_E = \|v_u\|_V \quad (2.9)$$

where v_u is the solution of the variational problem,

$$\begin{cases} v_u \in V \\ (v_u, \delta v)_V = b(u, \delta v) \quad \forall \delta v \in V \end{cases} \quad (2.10)$$

with $(\cdot, \cdot)_V$ denoting the inner product in the test space V .

Optimal test functions. Let $U_{hp} \subset U$ be a finite-dimensional space with a basis $e_j = e_{j, hp}$, $j = 1, \dots, N = N_{hp}$. For each basis *trial* function e_j , we introduce a corresponding *optimal test (basis) function* $\bar{e}_j \in V$ that realizes the supremum,

$$|b(e_j, \bar{e}_j)| = \sup_{\|v\|_V=1} |b(e_j, v)| \quad (2.11)$$

i.e. solves the variational problem,

$$\begin{cases} \bar{e}_j \in V \\ (\bar{e}_j, \delta v)_V = b(e_j, \delta v) \quad \forall \delta v \in V \end{cases} \quad (2.12)$$

The test space is now defined as the span of the optimal test functions, $\bar{V}_{hp} := \text{span}\{\bar{e}_j, j = 1, \dots, N\} \subset V$.

The Petrov-Galerkin discretization of the problem (2.1) with the optimal test functions takes the form:

$$\begin{cases} u_{hp} \in U_{hp} \\ b(u_{hp}, v_{hp}) = l(v_{hp}) \quad \forall v_{hp} \in \bar{V}_{hp} \end{cases} \quad (2.13)$$

It follows from the construction of the optimal test functions that the *discrete* inf-sup constant

$$\inf_{\|u_{hp}\|_E=1} \sup_{\|v_{hp}\|=1} |b(u_{hp}, v_{hp})| \quad (2.14)$$

is also equal to one. Consequently, Babuška's Theorem [2] implies that

$$\|u - u_{hp}\|_E \leq \inf_{w_{hp} \in U_{hp}} \|u - w_{hp}\|_E \quad (2.15)$$

i.e., the method delivers the *best approximation error* in the energy norm.

The construction of optimal test functions implies also that the global stiffness matrix is *symmetric and positive-definite*. Indeed,

$$b(e_i, \bar{e}_j) = (\bar{e}_i, \bar{e}_j)_V = (\bar{e}_j, \bar{e}_i)_V = b(e_j, \bar{e}_i) \quad (2.16)$$

Once the approximate solution has been obtained, the energy norm of the FE error $e_{hp} := u - u_{hp}$ is determined by solving again the variational problem

$$\begin{cases} v_{e_{hp}} \in V \\ (v_{e_{hp}}, \delta v)_V = b(u - u_{hp}, \delta v) = l(\delta v) - b(u_{hp}, \delta v) \quad \forall \delta v \in V \end{cases} \quad (2.17)$$

We shall call the solution $v_{e_{hp}}$ to the problem (2.17) the *error representation function* since we have

$$\|e_{hp}\|_E = \|v_{e_{hp}}\|_V \quad (2.18)$$

Notice that the energy norm of the error can be computed (approximately, see below) *without knowledge* of the exact solution. Indeed, the energy norm of the error is nothing else than a properly defined norm of the residual.

Approximate optimal test functions. In practice, the optimal test functions \bar{e}_j and the error representation function $v_{e_{hp}}$ are computed approximately using a sufficiently large “*enriched*” subspace $V_{hp} \subset V$. The optimal test space \bar{V}_{hp} is then a subspace of the enriched test space V_{hp} . For instance, if elements of order p are used, the enriched test space may involve polynomials of order $p + \Delta p$. The approximate optimal test space forms a proper subspace of the enriched space and should not be confused with the enriched space itself, though.

2.2 Petrov-Galerkin Method for Nonlinear Problems

While DPG is only directly applicable to linear problems, typical approaches used to solve most nonlinear partial differential equations involve some form of Newton-Raphson linearization; in other words, instead of solving a single nonlinear equation, a sequence of linear equations is solved in hope that those solutions will converge to the solution to the nonlinear problem.

Consider a nonlinear variational problem:

$$\begin{cases} \text{Find } u \in U \text{ such that} \\ b(u, v) = l(v), \quad \forall v \in V \end{cases} \quad (2.19)$$

where $b(u, v)$ is linear in v but not u , and $l \in V'$. By assuming $u = u_0 + \Delta u$, or that u is a small perturbation of some initial guess for the solution u_0 , we can linearize form b at u_0 ,

$$b(u, v) = b(u_0 + \Delta u, v) \approx b(u_0, v) + b_{u_0}(\Delta u, v) \quad (2.20)$$

where bilinear form $b_{u_0}(\Delta u, v)$ corresponds to the Gateaux derivative of nonlinear operator B associated with form $b(u, v)$,

$$B : U \rightarrow V', \quad \langle Bu, v \rangle = b(u, v), \quad \forall v \in V \quad (2.21)$$

Replacing the nonlinear form b in (2.19) with approximation (2.20), we obtain a linear variational problem for the increment Δu ,

$$b_{u_0}(\Delta u, v) = l(v) - b(u_0, v) =: l_{u_0}(v) \quad (2.22)$$

where both the bilinear form $b_{u_0}(\cdot, \cdot)$ and right hand side $l_{u_0}(v)$ depend in some way on the initial guess u_0 .

If we update our initial guess $u_1 = u_0 + \Delta u$, we can solve the linearized problem again with u_1 in place of u_0 and, continuing this way, generate a sequence of solutions u_n that converge to the solution to the

nonlinear problem. For most of this paper, we will denote an arbitrary term in this sequence as u , with Δu being an update to the previous Newton-Raphson solution u satisfying

$$b_u(\Delta u, v) = l_u(v) := l(v) - b(u, v) \quad (2.23)$$

where $b_u(\Delta u, v)$ depends on the previous solution u .

We can look at the problem using operator notation as well. If B denotes the nonlinear operator (2.21) corresponding to form $b(u, v)$, the original variational problem can be written in the operator form,

$$Bu = l. \quad (2.24)$$

The linearization of $b(u, v)$ then corresponds to the linearization

$$B(u + \Delta u) \approx Bu + B_u \Delta u, \quad (2.25)$$

where B_u is the Gateaux derivative of B at u ,

$$\langle B_u \Delta u, v \rangle = b_u(\Delta u, v). \quad (2.26)$$

Given some previous iterate u , our linearized problem in this notation is

$$B_u \Delta u = l - Bu \quad (2.27)$$

Measuring convergence

Since the Petrov–Galerkin method’s error representation function only measures the error associated with a given linear problem, we need measures of error for our nonlinear problem as well. Since the residual $f_u(v)$

$$f_u(v) := b(u, v) - l(v), \quad (2.28)$$

is a functional in V' , it is natural to measure it in the dual norm,

$$\|f_u(v)\|_{V'} = \sup_{v \in V} \frac{|f_u(v)|}{\|v\|_V} \quad (2.29)$$

Recalling that the Riesz operator is an isometry from V into its dual V' , we can invert the Riesz operator and compute the norm of the residual by finding v_f that satisfies

$$(v_{f_u}, \delta v) = f_u(\delta v), \quad \forall \delta v \in V \quad (2.30)$$

and taking $\|f_u\|_{V'} = \|v_{f_u}\|_V$.

Note that for nonlinear problems, given approximate solutions $u_{hp} \in U_{hp} \in U$, we cannot interpret the computable *nonlinear residual*

$$\|Bu_{hp} - l\|_{V'} = \sup_{v \in V} \frac{|b(u_{hp}, v) - l(v)|}{\|v\|_V} = \|f_{u_{hp}}(v)\|_{V'} \quad (2.31)$$

as the (energy) norm of the error $\|u - u_{hp}\|_E$ as we could for linear problems.

We are also interested in measuring the norm of our Newton-Raphson update. We have at our disposal the energy norm (in which PG is optimal) of Δu implied by the linearized problem,

$$\|\Delta u\|_E = \sup_{v \in V} \frac{|b_u(\Delta u, v)|}{\|v\|_V}. \quad (2.32)$$

It's important to recognize that the meaning of $\|\Delta u\|_E$ may be different from what is typically meant by the size of the Newton-Raphson update. The convergence of Newton-Raphson is usually measured by computing $\|\Delta u\|$ in some prescribed norm. Unlike typical norms (L_2 , H_1 , ℓ_p), the energy norm $\|\Delta u\|_E$ depends on the accumulated solution u and thus changes from step to step. What $\|\Delta u\|_E$ does tell us, however, is when our measure of error in the energy norm stabilizes. When $\|\Delta u_{hp}\|_E$ is small,

$$l_{u_{hp}}(v) - b_{u_{hp}}(\Delta u_{hp}, v) \approx l_{u_{hp}}(v) = l(v) - b(u_{hp}, v) \quad (2.33)$$

and our error representation function e_{hp} obeys

$$(e_{hp}, \delta v)_V = l_{u_{hp}}(\delta v) - b_{u_{hp}}(\Delta u_{hp}, \delta v) \approx l_{u_{hp}}(\delta v) = l(v) - b(u_{hp}, \delta v) \quad (2.34)$$

In other words, as the energy norm of Δu becomes small, both the error and the error representation function for the linearized problem tend towards the residual error and error representation function for the nonlinear problem.

$$\|\Delta u - \Delta u_{hp}\|_E = \|l_{u_{hp}} - Bu_{hp} - B_u \Delta u_{hp}\|_{V'} \geq \|l_{u_{hp}} - Bu_{hp}\|_{V'} - \|B_u \Delta u_{hp}\|_{V'} \quad (2.35)$$

Thus, given u , the exact solution to the nonlinear problem, Δu , the exact solution for a linearized problem, u_{hp} , the discrete approximate solution to the nonlinear problem (accumulated through a series of Newton-Raphson updates), and Δu_{hp} , the discrete approximate solution to a linear problem, we have three different quantities with which we can measure convergence:

1. the energy norm of our Newton-Raphson update, $\|\Delta u_{hp}\|_E$;
2. the discretization error in the energy norm for a given linearized problem $\|\Delta u - \Delta u_{hp}\|_E$;
3. the nonlinear residual $\|l(\cdot) - b(u, \cdot)\|_{V'} = \|Bu - l\|_{V'}$.

Note that the energy norm used in the first two quantities depends upon the accumulated solution u .

3 Burgers' Equation

In order to demonstrate the behavior of DPG, we study first its application to the 1-D viscous Burgers' equation, which first appeared in 1948 in J.M. Burgers' model for turbulence [12, 18], where he notes the

relationship between the model theory and shock waves. While Burgers' model for turbulence seems to have been forgotten, his equation has become very popular as a test case for computational fluid dynamics methods.

Burgers' equation shows a roughly similar structure to the compressible Navier Stokes equations. It is derivable from the Navier Stokes equations by assuming constant density, pressure, and viscosity, and is found in other aerodynamical applications as well. Most importantly, it shows typical features of shock-wave theory: the mathematical structure includes a nonlinear term tending to steepen the wave front and create shocks, and a higher-order viscous term that regularizes the equation and produces a dissipative effect on the solution near a shock. On a more physical side, the equation's solution demonstrates irreversibility in time, analogous to the irreversible flow of compressible fluids with shock discontinuities.

We consider the following initial boundary-value problem.

$$\left\{ \begin{array}{l} \text{Find } u(x, t) \text{ such that} \\ \frac{\partial u}{\partial t} - \epsilon \frac{\partial^2 u}{\partial x^2} + \frac{\partial}{\partial x} \left(\frac{1}{2} u^2 \right) = 0 \\ u(-\frac{1}{2}, t) = 1, \quad u(\frac{1}{2}, t) = -1 \\ u(x, 0) = -2x \end{array} \right. \quad (3.36)$$

It is known for the inviscid case that after a finite time ($t = \frac{1}{2}$) the solution forms a shock at $x = 0$ [12]. The viscous solution behaves similarly, forming a smeared shock and eventually reaching its steady-state governed by the following nonlinear boundary-value problem.

$$\left\{ \begin{array}{l} \text{Find } u(x) \text{ such that} \\ -\epsilon \frac{d^2 u}{dx^2} + \frac{d}{dx} \left(\frac{1}{2} u^2 \right) = 0 \\ u(-\frac{1}{2}) = 1, \quad u(\frac{1}{2}) = -1 \end{array} \right. \quad (3.37)$$

3.1 Sensitivity with respect to boundary condition data

We can use separation of variables to find the steady-state solution. Integrating the Burgers equation in x , we get

$$-\epsilon \frac{du}{dx} + \frac{1}{2} u^2 = C$$

Based on the expected form of the solution, we assume that the integration constant is positive, $C = \frac{1}{2} c^2$, $c > 0$. This leads to separation of variables

$$\frac{2\epsilon du}{u^2 - c^2} = dx$$

and, upon integration,

$$\frac{\epsilon}{c} \ln \left| \frac{u - c}{u + c} \right| = x - d$$

ϵ	d	Δu_1	Δu_2
0.100	-0.25	-0.151716360042487E-000	-1.105557273847199E-003
0.100	0.00	-1.338570184856971E-002	-1.338570184856971E-002
0.100	0.25	-1.105557273847199E-003	-0.151716360042487E-000
0.010	-0.25	-2.777588772954229E-011	-5.357273923616156E-033
0.010	0.00	-3.857499695927836E-022	-3.857499695927836E-022
0.010	0.25	-5.357273923616156E-033	-2.777588772954229E-011
0.001	-0.25	-5.338380431082553E-109	0.000000000000000E+000
0.001	0.00	-1.424915281348257E-217	-1.424915281348257E-217
0.001	0.25	0.000000000000000E+000	-5.338380431082553E-109

Table 1: Perturbation of the boundary conditions data for $c = 1$ and various values of ϵ and d .

where d is another integration constant. Assuming that the solution is decreasing, we obtain,

$$\frac{c - u}{c + u} = e^{\frac{\epsilon}{c}(x-d)}$$

Constant c can now be interpreted now as the value of the (extension of the) solution at $x = -\infty$ ($-c$ is the value at ∞), and constant d determines the location of the shock, i.e. the point where u vanishes.

We assume now a possible slight perturbation of the boundary conditions,

$$u\left(-\frac{1}{2}\right) = u_1 \approx 1, \quad u\left(\frac{1}{2}\right) = -u_2 \approx -1$$

Rather than attempting to determine the integration constants c, d in terms of boundary data u_1, u_2 , we represent u_1, u_2 in terms of c, d instead,

$$\begin{cases} u_1 = c \frac{1 - \beta}{1 + \beta}, & \beta = e^{-\frac{\epsilon}{c}(1/2+d)} \\ u_2 = c \frac{1 - \gamma}{1 + \gamma}, & \gamma = e^{-\frac{\epsilon}{c}(1/2-d)} \end{cases}$$

Table 1 shows the perturbations of u_1, u_2 from 1, for $c = 1$, $\epsilon = 0.1, 0.01, 0.001$, and $d = 0, -0.25, 0.25$. Starting with $\epsilon = 0.001$, the perturbations of the boundary data are beyond the machine precision.

Thus, for all practical purposes, we are attempting to solve numerically a problem with multiple solutions. Without introducing an additional mechanism for selecting the solution with shock at $x = 0$, we have little chance to converge to the “right” solution with the Newton-Raphson iterations.

3.2 Shock width

While the solution of the inviscid Burgers equation manifests a shock in the form of a discontinuous solution, the addition of viscosity “smears” the discontinuity, resulting in a continuous solution displaying high gradients near the shock.

Let u_L and u_R represent the values of the solution at the left and right boundaries, respectively, and assume the inviscid solution's discontinuity lies directly in the middle of the interval, at $x = x^*$. We can then study the smearing effect of the viscosity on the shock by examining the *shock width* δ_s , defined to be the distance in x that the maximum slope of u (which we can assume occurs at $x = 0$, the midpoint of our interval) takes to traverse the difference between u_L and u_R ,

$$\delta_s = \frac{u_R - u_L}{u'(x^*)} \quad (3.38)$$

The exact solution to the viscous Burgers equation on $(-\infty, \infty)$ is given in [3] as

$$u(x) = \frac{u_R \exp \left[\left(\frac{u_L - u_R}{2\nu} \right) x \right] + u_L}{\exp \left[\left(\frac{u_L - u_R}{2\nu} \right) x \right] + 1}. \quad (3.39)$$

If we use this, we can see that the shock width for Burgers equation is

$$\delta_s = \frac{8\nu}{u_L - u_R}. \quad (3.40)$$

If we assume $u_L = 1$, $u_R = -1$, the shock width just reduces to $\delta_s = 4\nu$.

3.3 The DPG Method for Burgers' Equation

Recall that the stationary Burgers' equation on $[0, 1]$ is ¹

$$1/2(u^2)_{,x} = (\nu u_{,x})_{,x}. \quad (3.41)$$

For boundary conditions $u(0) = 1$ and $u(1) = -1$, the solution to this equation develops shocks whose width depends on ν .

We begin by rewriting Burgers' equation as a system of first order equations,

$$\begin{aligned} \frac{1}{\nu} \sigma - u_{,x} &= 0 \\ \sigma_{,x} - \left(\frac{u^2}{2} \right)_{,x} &= 0 \end{aligned}$$

Given an element K with boundary ∂K , we multiply the equations with test functions τ and v , integrate over K , and integrate by parts to arrive at the variational form of the equations,

$$\begin{aligned} -u\tau|_{\partial K} + \int_K \frac{1}{\nu} \sigma \tau + u\tau_{,x} &= 0 \\ \left[\sigma v - \left(\frac{u^2}{2} \right) v \right]_{\partial K} + \int_K -\sigma v_{,x} + \left(\frac{u^2}{2} \right) v_{,x} &= 0 \end{aligned}$$

¹For convenience, we shift coordinates to $(0, 1)$ when solving the problem numerically.

After linearization, we obtain the variational formulation for the linearized equations,

$$\begin{aligned} \int_K \frac{1}{\nu} \Delta \sigma \tau - \Delta \hat{u} \tau|_{x_k}^{x_{k+1}} + \int_K \Delta u \tau_{,x} &= - \int_K \frac{1}{\nu} \sigma \tau + \hat{u} \tau|_{x_k}^{x_{k+1}} - \int_K u \tau_{,x} \\ \Delta \hat{\sigma} v|_{x_k}^{x_{k+1}} - (\hat{u} \Delta \hat{u}) v|_{x_k}^{x_{k+1}} + \int_K (u \Delta u - \Delta \sigma) v_{,x} &= - (\hat{\sigma} - \hat{u}^2/2) v|_{x_k}^{x_{k+1}} + \int_K (\sigma - u^2/2) v_{,x} \end{aligned}$$

Fluxes \hat{u} and $\hat{\sigma}$ and their increments $\Delta \hat{u}$ and $\Delta \hat{\sigma}$, are identified as independent unknowns.

3.3.1 Test space

For our test functions, we use the scaled H_1 inner product introduced in [15]

$$(v, \delta v) = \int_{x_{k-1}}^{x_k} (v' \delta v' + v \delta v) \alpha(x) dx \quad (3.42)$$

where $\alpha(x)$ is some scaling parameter. In our case, we let $\alpha(x)$ be equal to

$$\alpha(x) = \begin{cases} x/x_L, & x \leq x_L \\ 1 - x/x_R, & x \geq x_R \\ 1, & \text{otherwise} \end{cases} \quad (3.43)$$

in order to de-emphasize the error measure near the boundaries, where we expect the solution to vary very little. In the presented numerical experiments, we set $x_L = .1$ and $x_R = .9$.

3.3.2 Adaptive strategy

When adapting and iterating Newton-Raphson at the same time, there is a choice to be made in whether to adapt the mesh first and then perform Newton-Raphson iterations, or to do Newton-Raphson until converged, and then adapt.

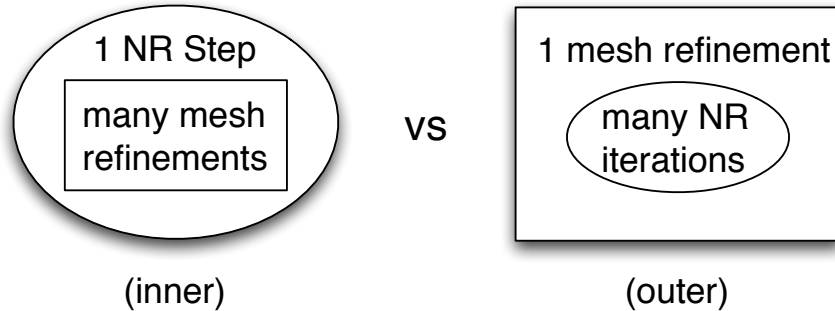


Figure 1: Inner vs. outer ordering of Newton-Raphson and adaptivity

This choice actually corresponds to the order in which we discretize/linearize. The linearization process can be done in two ways; we can consider discretizing the nonlinear equations first, then linearizing the

	Nonlinear		Linearized
Continuous	$Bu = l$	\Rightarrow	$B_u \Delta u = l - Bu$
	\Downarrow		\Downarrow
Discrete	$B_{hp} u_{hp} = l_{hp}$	\Rightarrow	$B_{u_{hp}} \Delta u_{hp} = l_{hp} - Bu_{hp}$

Figure 2: Two different ways to arrive at a discrete linearized problem using operator notation.

nonlinear discrete problem, or linearizing the continuous problem first, then discretizing the continuous linearized problem.

Fig. 3 shows how reversing these two forms of linearization corresponds to our two choices concerning the order of the adaptivity and Newton-Raphson loops. Doing Newton-Raphson on the outside and adaptivity on the inside (Fig. 3(a)) is equivalent to solving each continuous linearized problem “exactly” (in the sense of minimizing discretization error).

Alternatively, doing adaptivity on the outside and Newton-Raphson on the inside (Fig. 3(b)) corresponds to refining on the nonlinear problem. This approach uses discrete linearized solutions to approximate the nonlinear discrete solution; essentially solving the nonlinear problem “exactly” on a fixed/given mesh (in the sense of minimizing $\|\Delta\|_E$).

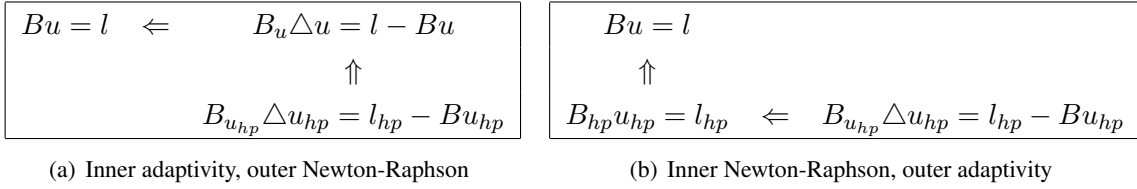


Figure 3: Inner vs. outer ordering of Newton-Raphson and adaptivity

Motivation for the former ordering comes in part from the stability of DPG; since DPG is proven to provide optimality for the linear problem, it is possible to completely resolve each linearized step. Numerical experiments with Burgers’ equation on fixed meshes also showed that Newton-Raphson tended to stabilize ($\|\Delta u\|_E \approx 0$) fastest when the element size was smaller than the shock width—in other words, when the mesh could resolve the shock. Another motivation is the dependence of the energy norm on the previous solution u ; since this is the norm in which the solution is optimal, it is likely that resolving the previous solution more closely could eliminate the effect of discretization error upon the norm.

However, in practice, the cost of resolving each linearized problem makes the process of converging to the nonlinear solution much more expensive. Extra refinements are done in order to resolve the intermediate Newton-Raphson iterates but are unnecessary to represent the final shock solution. The obvious solution would be to implement unrefinements, but there will be some information accumulated from previous iterates lost in this process. Another drawback to resolving each linearized solution is that the degrees of freedom (dofs) needed to resolve an intermediate Newton-Raphson step may be greater than the total degrees of freedom needed to support the final converged solution. For this paper, we implement refinements using a Newton-Raphson loop on the inside and adaptivity on the outside.

3.3.3 *hp*-adaptive strategy

The previous papers used a so called “poor man’s greedy *hp* algorithm” summarized below to guide the mesh refinements.

The strategy reflects old experiments with boundary layers [16], and the rigorous approximability results of

```

Set  $\delta = 0.5$ 
do while  $\delta > 0.1$ 
  solve the problem on the current mesh
  for each element  $K$  in the mesh
    compute element error contribution  $e_K$ 
  end of loop through elements
  for each element  $K$  in the mesh
    if  $e_K > \delta^2 \max_K e_K$  then
      if new  $h \geq \epsilon$  then
         $h$ -refine the element
      elseif new  $p \leq p_{max}$  then
         $p$ -refine the element
      endif
    endif
  end of loop through elements
  if (new  $N_{dof} = \text{old } N_{dof}$ ) reset  $\delta = \delta/2$ 
end of loop through mesh refinements

```

Figure 4: “Poor-man’s” *hp*-adaptivity for shock problems.

Schwab and Suri [23] and Melenk [20] on optimal *hp* discretizations of boundary layers: we proceed with h -refinements until the diffusion scale ϵ is reached and then continue with p -refinements.

For nonlinear problems, we adopt the same algorithm, but interpret the line “solve the problem on the current mesh” as solving the nonlinear problem for that given mesh. In other words, we iterate Newton-Raphson on that mesh until $\|\Delta u\|_E$ is smaller than a certain tolerance, and we consider that the solution of the nonlinear problem. Note that for a solution converged in Newton-Raphson, since on the K th element both the nonlinear residual $\|l(\cdot) - b(u_{hp}, \cdot)\|_{V'}$ and the error $\|\Delta u - \Delta u_{hp}\|_E$ are equivalent to the element error e_K , using the error to guide refinements should decrease the nonlinear residual and take us closer to the exact solution u of the nonlinear problem.

With this, our strategy for inner loop Newton-Raphson and outer loop adaptivity is

```

do while  $\|Bu - l\|_{V'} > \epsilon$ 
  do while  $\|\Delta u\|_E > tol$ 
    solve  $b_u(\Delta u, v) = l(v) - b(u, v)$ 
    update  $u := u + \Delta u$ 
  end of Newton-Raphson loop
  do one hp refinement using the "poor man" algorithm
end of refinement loop

```

Figure 5: Inner Newton-Raphson refinement algorithm.

3.4 Numerical results

3.4.1 Viscous Burgers

Using outer adaptivity with inner Newton-Raphson (so that refinements are only placed after a solution's Newton-Raphson iterates have converged on a given mesh) coupled with our “poor-man’s” *hp*-adaptive strategy, we apply DPG to the viscous Burgers’ equation.

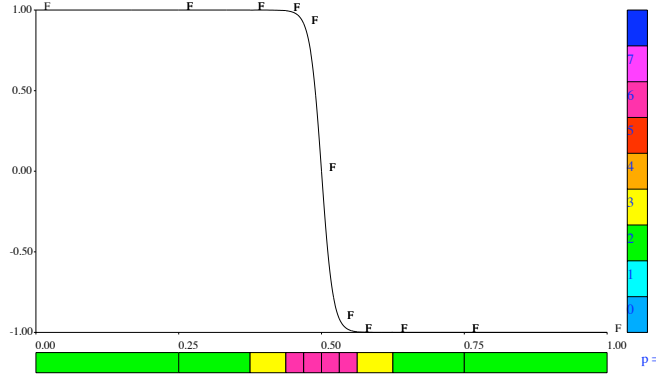
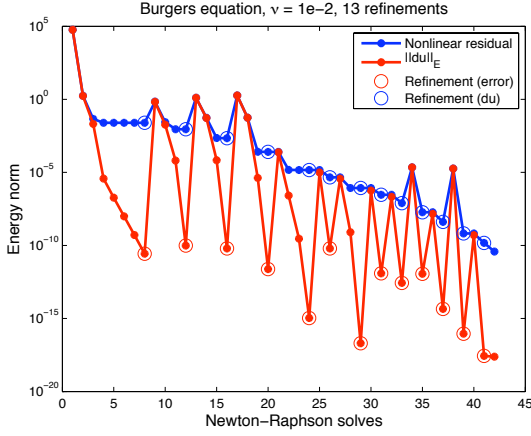


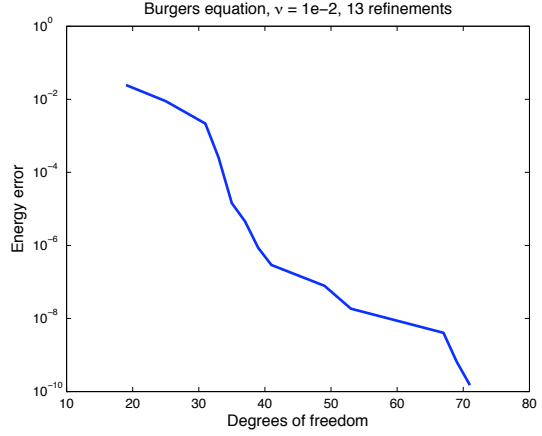
Figure 6: Burgers equation with $\nu = 10^{-2}$ and initial mesh of 2 elements. Solution after nine refinements, with $\|\Delta u\|_E = 1.28 \times 10^{-13}$ and nonlinear residual error of 2.33×10^{-6} .

For an illustration of how inner Newton-Raphson/outer adaptivity behaves, we examine how both $\|\Delta u\|_E$ and the nonlinear residual error change as we iterate Newton-Raphson and add refinements.

The error plots in Fig. 7, Fig. 8, and Fig. 9 show the progression of both $\|\Delta u\|_E$ and the nonlinear residual error with Newton-Raphson iterates. The circled points are iterates of Newton-Raphson where $\|\Delta u\|_E$ is smaller than a given tolerance and, at the next point, a refinement is done. $\|\Delta u\|_E$ decreases until a refinement is done, at which point both the residual and $\|\Delta u\|_E$ change again.



(a) Both $\|\Delta u\|$ and nonlinear residual error.



(b) Nonlinear residual error

Figure 7: Burgers' equation error plots for $\nu = 10^{-2}$

The increase in both $\|\Delta u\|_E$ and the nonlinear residual after a refinement actually comes in two parts. During refinement, an element is broken into two new elements. The previous solution u over the original unbroken element is reproduced using the degrees of freedom on the two new elements; however, the previous solution's flux at the boundary between the two new elements remains to be initialized. In this paper, we've simply set those values equal to the pointwise values of the solutions on the original element. However, it turns out that this change in itself causes the nonlinear residual to change.

We examine the simplest case of a pure convection problem to illustrate the point. Suppose we wish to solve the initial-value problem,

$$u' = 0, \quad u(0) = u_0 \quad (3.44)$$

with the corresponding variational form,

$$-\int_{x_{j-1}}^{x_j} uv' + \hat{u}v|_{x_{j-1}}^{x_j} = 0, \quad (3.45)$$

over the j th element. For such an element in the interior, where the source is 0, we have that the error representation function v satisfies

$$\int_{x_{j-1}}^{x_j} v' \delta v' + v \delta v = \int_{x_{j-1}}^{x_j} u \delta v' - \hat{u} \delta v|_{x_{j-1}}^{x_j} \quad (3.46)$$

By integrating by parts again, we can retrieve the classical problem corresponding to the above variational problem.

$$\begin{cases} -v'' + v &= -u' \\ v'(x_j) &= u(x_j) - \hat{u}(x_j) \\ -v'(x_{j-1}) &= \hat{u}(x_{j-1}) - u(x_j) \end{cases} \quad (3.47)$$

Now, assuming the element is broken at $x_{j-1/2}$, we aim to assign the flux $\hat{u}(x_{j-1/2})$ such that the error representation function is the same as before being broken. In other words, we seek to assign $\hat{u}(x_{j-1/2})$ such that the new error representation functions on $[x_{j-1}, x_{j-1/2}]$ and $[x_{j-1/2}, x_j]$ are identical to the error representation function over $[x_{j-1}, x_j]$.

The error representation function over $[x_{j-1}, x_{j-1/2}]$ satisfies

$$\int_{x_{j-1}}^{x_{j-1/2}} v' \delta v' + v \delta v = \int_{x_{j-1}}^{x_{j-1/2}} u \delta v' - \hat{u} \delta v|_{x_{j-1}}^{x_{j-1/2}} \quad (3.48)$$

If we integrate by parts over $[x_{j-1}, x_{j-1/2}]$, we can recover the classical problem

$$\begin{cases} -v'' + v = -u' \\ v'(x_{j-1/2}) = u(x_{j-1/2}) - \hat{u}(x_{j-1/2}) \\ -v'(x_{j-1}) = \hat{u}(x_{j-1}) - u(x_{j-1}) \end{cases} \quad (3.49)$$

Doing the same over $[x_{j-1/2}, x_j]$, we get

$$\begin{cases} -v'' + v = -u' \\ -v'(x_{j-1/2}) = \hat{u}(x_{j-1/2}) - u(x_{j-1/2}) \\ v'(x_j) = \hat{u}(x_j) - u(x_j) \end{cases} \quad (3.50)$$

implying that

$$\hat{u}(x_{j-1/2}) = u(x_{j-1/2}) - v'(x_{j-1/2}) \quad (3.51)$$

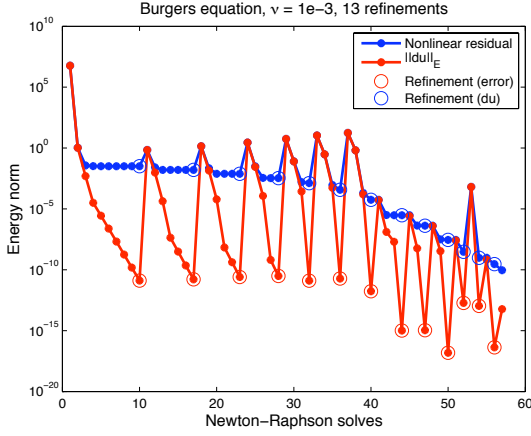
and leaving us with the non-intuitive result that, in order to keep the error the same, the flux at a new element boundary must be initialized using not only the field variable within the element, but the derivative of the error function as well. Thus, initializing the flux any other way may change the error. An analogous lesson holds for nonlinear problems; initializing the previous solution flux just using pointwise values of the solution means that the nonlinear residual can change. The jump in nonlinear residual after a refinement actually happens in between one Newton-Raphson solve and the next through our process of assigning the flux for a refined element.

Notice in Fig. 9 (for $\nu = 1e - 4$) that between the 70th and 80th Newton-Raphson solve, $\|\Delta u\|_E$ no longer decreases monotonically between refinements near the end, and instead oscillates before decreasing. We believe that this is a consequence of the sensitivity to boundary conditions exhibited by Burgers' equation that was discussed earlier.

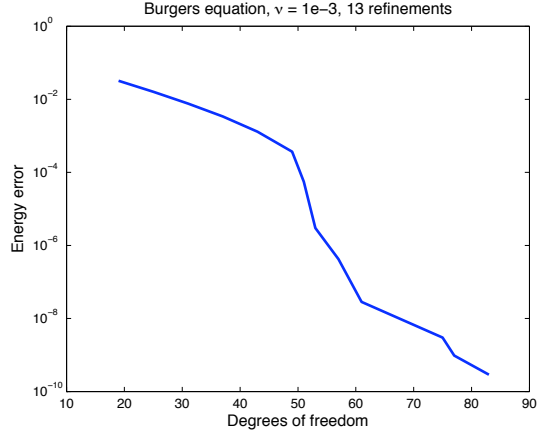
3.4.2 Smaller shock widths

Due to issues with conditioning of the stiffness matrix (which in turn are due to large gradients in the solution for small shock widths), we follow [15] and introduce a mesh-dependent norm

$$(v, \delta v) = \int_{x_{k-1}}^{x_k} (h_k v' \delta v' + v \delta v) \alpha(x) dx \quad (3.52)$$

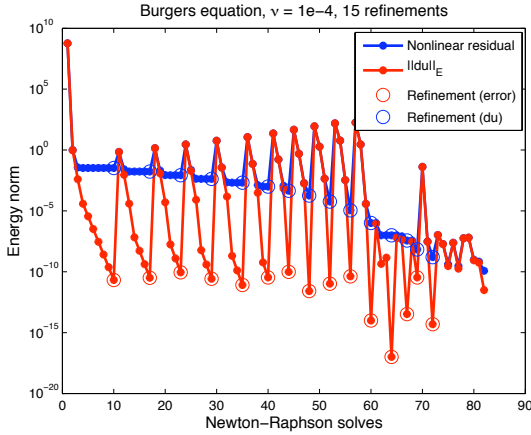


(a) Both $\|\Delta u\|$ and nonlinear residual error.

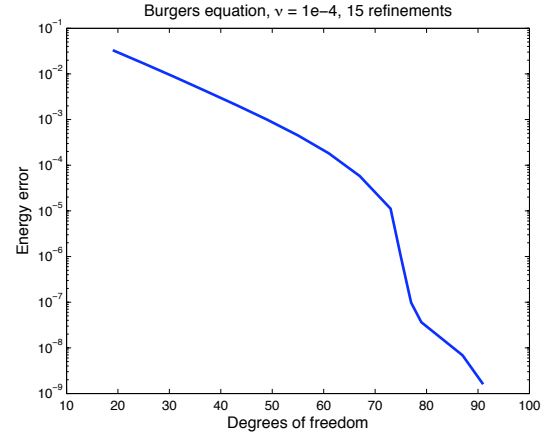


(b) Nonlinear residual error

Figure 8: Burgers' equation error plots for $\nu = 10^{-3}$



(a) Both $\|\Delta u\|$ and nonlinear residual error.



(b) Nonlinear residual error

Figure 9: Burgers' equation error plots for $\nu = 10^{-4}$

where h_k is the k th element size. This allows us to resolve shocks for ν as small as 10^{-11} .

Unfortunately, for ν smaller than 10^{-4} , we begin to see effects from Burgers' problem sensitivity to boundary conditions; as we resolve the shock more fully, the size of the Newton step $\|\Delta u\|_E$ begins to oscillate, indicating the solution is, at least to double precision arithmetic, non-unique. Thus, it is no longer meaningful to talk about convergence to a solution. Even if $\|\Delta u\|_E$ and the nonlinear residual are both small in one Newton-Raphson step, taking another Newton-Raphson step may introduce enough floating point error to cause $\|\Delta u\|_E$ and the nonlinear residual to change drastically.

As with convection-dominated diffusion, we see in Fig. 11(b) when our diffusion parameter is $O(10^{-11})$ that our error function becomes discontinuous. Since the error function was proven to be continuous in [15],

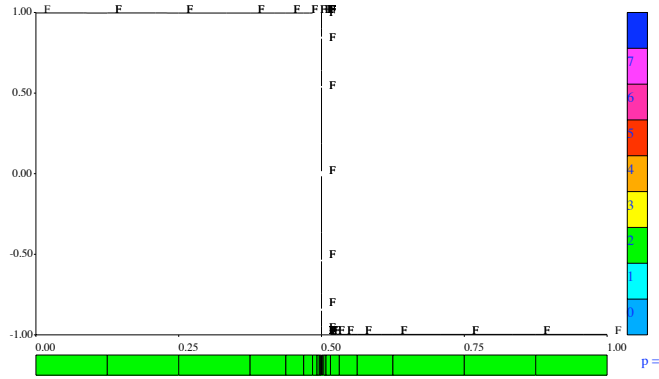
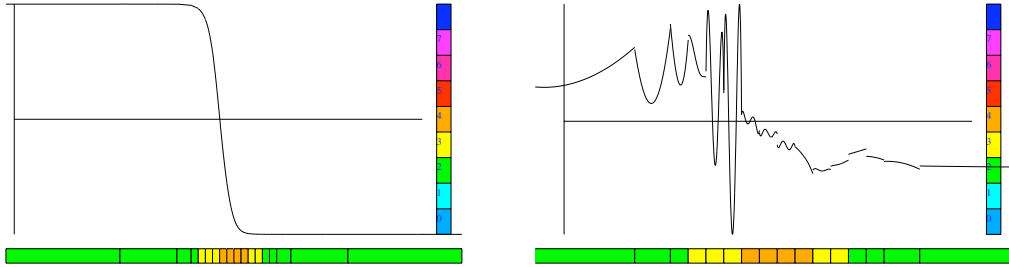


Figure 10: Zoomed out Burgers' equation solution u for $\nu = 10^{-11}$



(a) Zoomed in u for $\nu = 10^{-11}$

(b) Zoomed in error function for $\nu = 10^{-11}$. The discontinuity indicates that finite precision arithmetic is starting to affect our solution.

this gives some indication that $\nu = 10^{-11}$ is the smallest resolvable shock width using double precision arithmetic.

3.4.3 Inviscid Burgers

The inviscid Burgers equation is given as

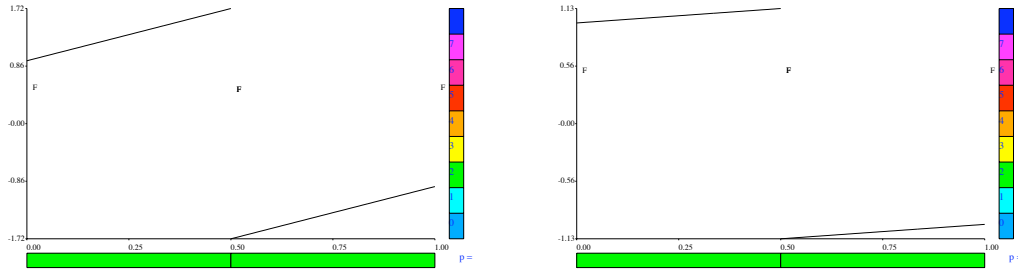
$$1/2(u^2)_{,x} = 0 \quad (3.53)$$

The linearized variational form is then

$$\frac{1}{2}[u^2v]\Big|_{\partial K} - \int_K u \Delta u v_x = \int_K 1/2(u^2)v_x$$

where the $\frac{1}{2}[u^2v]$ term is identified as a new flux unknown.

Unlike the viscous Burgers equation, the inviscid case is a first order system, without a higher order viscous term to smooth out a shock, so the solution exhibits a discontinuity. We tested DPG on the inviscid Burgers' equation to see how it would handle actual discontinuities, which can develop even in the case of the full Navier-Stokes equations².



(c) First Newton-Raphson iterate

(d) Second Newton-Raphson iterate

Figure 11: First and second Newton-Raphson iterates for inviscid Burgers

DPG handles the discontinuity very well, converging with both nonlinear error and $\|\Delta u\|_E$ to under machine precision in 6 Newton-Raphson iterates.

We converge to an exact solution, a step function from $[-1, 1]$ with the discontinuity located in the middle. The steady-state inviscid Burgers' equation has infinitely many solutions, and the location of the shock very sensitive to the initial data. With an even number of elements and the interval mid-point exactly at an element boundary, DPG seems to perform well.

Unfortunately, we note that in 1D, the mesh makes achieving the exact solution almost trivial. For an even number of elements, the discontinuity lies right at the boundary between two elements, while for an odd number of elements, a single refinement to the middle element will put an element boundary right at the discontinuity as well. For uniform refinements of initial meshes with odd numbers of elements, we can see in Fig. 13 that the overshoot and undershoot near $x = 1/2$ is localized to one element. We plan to study higher dimensional discontinuous solutions, where more complex shock structures make it much less likely that shocks will lie exactly on element boundaries.

²Contact discontinuities.

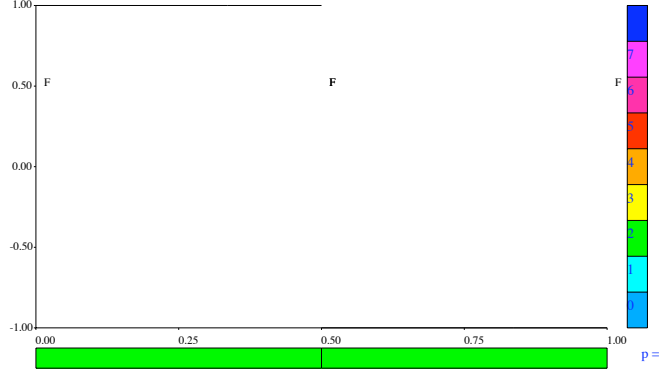


Figure 12: The fifth NR iterate. Both $\|\triangle u\|_E$ and nonlinear error are 8.223×10^{-11}

4 Navier-Stokes

4.1 Stationary Shock Formulation

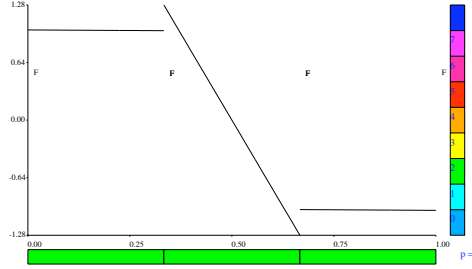
We consider the compressible Navier-Stokes equations on a stationary, one-dimensional shock.³ Under the assumption that the fluid is inviscid, the Euler equations admit a discontinuous (shock) solution. However, a consequence of the second law of thermodynamics is that no fluid is entirely inviscid; with viscous effects, we expect to see graphs with large gradients and a “smeared” shock.

4.1.1 Physical Assumptions

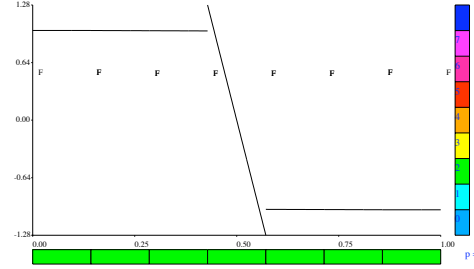
Our derivation makes the following physical assumptions:

- the system is steady,
- the only contributions to energy are mechanical and thermal energy,
- Fourier’s law of heat conduction (with constant κ) $\frac{\partial q}{\partial x} = -\kappa \frac{\partial T}{\partial x}$ applies,
- the fluid is a perfect gas—that is, $p = \rho RT$, and
- the fluid is Newtonian; $\tau_{\text{visc}} = (2\mu + \lambda) \frac{\partial u}{\partial x}$, where μ and λ are temperature-dependent fluid and bulk viscosity terms.

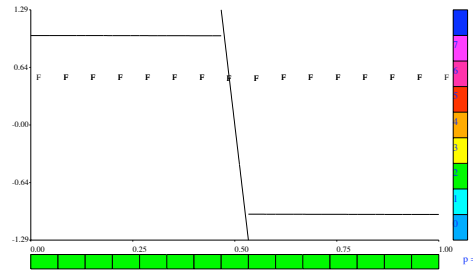
³We use a moving reference in which the shock is stationary.



(a) Inviscid Burgers on a 3 element mesh



(b) Inviscid Burgers on a 7 element mesh



(c) Inviscid Burgers on a 15 element mesh

Figure 13: Converged solutions for inviscid Burgers on meshes with odd numbers of elements.

4.1.2 Boundary Conditions

To determine appropriate boundary conditions for our problem, we consider the system as inviscid—the Navier-Stokes equations then reduce to the Euler equations. The result is a set of conditions known as the *normal shock conditions* (also known as the Rankine-Hugoniot jump conditions). Together with the perfect gas law and the shock strength equation ([1], p.90), we then have the following relations:

$$\begin{aligned}
\rho_a u_a &= \rho_b u_b \\
\rho_a u_a^2 + p_a &= \rho_b u_b^2 + p_b \\
\rho_a u_a \left(E_a + \frac{p_a}{\rho_a} \right) &= \rho_b u_b \left(E_b + \frac{p_b}{\rho_b} \right) \\
p = (\gamma - 1) \rho E_{\text{thermal}} &= (\gamma - 1) \rho \left(E - \frac{u^2}{2} \right) \\
u_a^2 &= 1 + \frac{\gamma + 1}{2\gamma} \left(\frac{p_b}{p_a} - 1 \right)
\end{aligned}$$

where γ is the ratio of specific heats, and subscripts a and b denote values of the corresponding quantities at the endpoints of the interval (a, b) in which the problem is formulated.

We then fix the values of ρ_a (density at the left end) and u_a (the Mach number we would like to impose on the left), and determine the following formulas:

$$\begin{aligned}
p_a &= \frac{\rho_a}{\gamma} \\
p_b &= p_a \left(1 + \frac{2\gamma}{\gamma + 1} (u_a^2 - 1) \right) \\
\rho_b &= \rho_a \frac{(\gamma - 1) + (\gamma + 1) \frac{p_b}{p_a}}{(\gamma + 1) + (\gamma - 1) \frac{p_b}{p_a}} \\
u_b &= \frac{\rho_a u_a}{\rho_b} \\
E_a &= \frac{u_a^2}{2} + \frac{p_a}{(\gamma - 1) \rho_a} \\
E_b &= \frac{u_b^2}{2} + \frac{p_b}{(\gamma - 1) \rho_b}
\end{aligned}$$

As we will see, once we have derived the linearized variational form, there is a small subtlety in imposing these boundary conditions using the DPG method, because DPG applies boundary conditions to the fluxes.

4.1.3 Basic Equations

We begin with the non-dimensionalized Navier-Stokes equations in 1D over $x \in [0, 1]$, choosing density ρ , velocity u and total energy e for unknowns. Assuming steady-state, a Newtonian fluid, Fourier's law, and constant Prandtl number, the conservation equations are

$$\begin{aligned}
(\rho u)_{,x} &= 0 \\
(\rho u^2)_{,x} + (p)_{,x} - \frac{1}{\text{Re}} (\tau)_{,x} &= 0 \\
(\rho e u)_{,x} - \frac{1}{\text{Re Pr}(\gamma - 1)} (\mu(T)_{,x})_{,x} + (p u)_{,x} - \frac{1}{\text{Re}} (\tau u)_{,x} &= 0
\end{aligned}$$

with constitutive equations

$$\begin{aligned} T &= \gamma(\gamma - 1) \left(e - \frac{u^2}{2} \right) \\ p &= \frac{\rho T}{\gamma} \\ \tau &= (2\mu + \lambda)(u)_{,x} \end{aligned}$$

Rewriting this as a system of five first-order equations, we obtain:

$$\begin{aligned} (\rho u)_{,x} &= 0 \\ \left(\rho u^2 + (\gamma - 1)\rho \left(e - \frac{u^2}{2} \right) - \frac{1}{\text{Re}} \tau \right)_{,x} &= 0 \\ \left(\rho e u - \frac{\gamma}{\text{Re Pr}} w + (\gamma - 1)\rho u \left(e - \frac{u^2}{2} \right) - \frac{1}{\text{Re}} \tau u \right)_{,x} &= 0 \\ \tau - (2\mu + \lambda)(u)_{,x} &= 0 \\ w - \mu \left(e - \frac{u^2}{2} \right)_{,x} &= 0 \end{aligned}$$

and, if we define the fluxes f_i as

$$\begin{aligned} f_1(\vec{u}) &= \rho u \\ f_2(\vec{u}) &= \rho u^2 + (\gamma - 1) \left(e - \frac{u^2}{2} \right) - \frac{1}{\text{Re}} \tau \\ f_3(\vec{u}) &= \rho e u - \frac{\gamma}{\text{Re Pr}} w + (\gamma - 1)\rho u \left(e - \frac{u^2}{2} \right) - \frac{1}{\text{Re}} \tau u \\ f_4(\vec{u}) &= \nu u \\ f_5(\vec{u}) &= \mu \left[e - \frac{u^2}{2} \right] \end{aligned}$$

where $\nu = 2\mu + \lambda$, our five equations become

$$\begin{aligned} f_1(\vec{u})_{,x} &= 0 \\ f_2(\vec{u})_{,x} &= 0 \\ f_3(\vec{u})_{,x} &= 0 \\ \tau - f_4(\vec{u})_{,x} &= 0 \\ w - f_5(\vec{u})_{,x} &= 0. \end{aligned}$$

4.1.4 Variational Formulation

After multiplying by test functions v_1, \dots, v_5 and integrating by parts, we arrive at our nonlinear variational form

$$\begin{aligned}
\hat{f}_1 v_1 \Big|_{\partial K} - \int_K f_1(\vec{u}) v_{1,x} &= 0 & \forall v_1 \\
\hat{f}_2 v_2 \Big|_{\partial K} - \int_K f_2(\vec{u}) v_{2,x} &= 0 & \forall v_2 \\
\hat{f}_3 v_3 \Big|_{\partial K} - \int_K f_3(\vec{u}) v_{3,x} &= 0 & \forall v_3 \\
- \hat{f}_4 v_4 \Big|_{\partial K} + \int_K \tau v_4 + f_4(\vec{u}) v_{4,x} &= 0 & \forall v_4 \\
- \hat{f}_5 v_5 \Big|_{\partial K} + \int_K w v_5 + f_5(\vec{u}) v_{5,x} &= 0 & \forall v_5
\end{aligned}$$

where boundary fluxes \hat{f}_i have been identified as new unknowns.

4.1.5 Linearization

If we linearize both f_i and \hat{f}_i and rearrange terms, we get

$$\begin{aligned}
\Delta \hat{f}_1 v_1 \Big|_{\partial K} - \int_K \Delta f_1 v_{1,x} &= \int_K \bar{f}_1 v_{1,x} - \bar{\hat{f}}_1 v_1 \Big|_{\partial K} \\
\Delta \hat{f}_2 v_2 \Big|_{\partial K} - \int_K \Delta f_2 v_{2,x} &= \int_K \bar{f}_2 v_{2,x} - \bar{\hat{f}}_2 v_2 \Big|_{\partial K} \\
\Delta \hat{f}_3 v_3 \Big|_{\partial K} - \int_K \Delta f_3 v_{3,x} &= \int_K \bar{f}_3 v_{3,x} - \bar{\hat{f}}_3 v_3 \Big|_{\partial K} \\
- \Delta \hat{f}_4 v_4 \Big|_{\partial K} + \int_K \Delta \tau v_4 + \Delta f_4 v_{4,x} &= \hat{f}_4 v_4 \Big|_{\partial K} - \int_K \bar{\tau} v_4 + \bar{f}_4 v_{4,x} \\
- \Delta \hat{f}_5 v_5 \Big|_{\partial K} + \int_K \Delta w v_5 + \Delta f_5 v_{5,x} &= \hat{f}_5 v_5 \Big|_{\partial K} - \int_K \bar{w} v_5 + \bar{f}_5 v_{5,x}
\end{aligned}$$

where our flux updates Δf_i are

$$\begin{aligned}
\Delta f_1 &= \Delta \rho \bar{u} + \Delta u \bar{\rho} \\
\Delta f_2 &= 2\Delta u \bar{u} \bar{\rho} + \Delta \rho \bar{u}^2 - \frac{1}{\text{Re}} \Delta \tau \\
&\quad + (\gamma - 1) \left(\Delta \rho \left(\bar{e} - \frac{\bar{u}^2}{2} \right) + \bar{\rho} (\Delta e - \Delta u \bar{u}) \right) \\
\Delta f_3 &= (\Delta \rho \bar{u} + \Delta u \bar{\rho}) \bar{e} + \bar{\rho} \bar{u} \Delta e - \frac{\gamma}{\text{RePr}} \Delta w \\
&\quad + (\gamma - 1) \left[\bar{\rho} \bar{u} (\Delta e - \Delta u \bar{u}) + (\rho \Delta u + u \Delta \rho) \left(e - \frac{u^2}{2} \right) \right] \\
&\quad - \frac{1}{\text{Re}} (\Delta \tau \bar{u} + \Delta u \bar{\tau}) \\
\Delta f_4 &= \nu \Delta u \\
\Delta f_5 &= (\mu (\Delta e - \Delta u \bar{u}))
\end{aligned}$$

and our accumulated Newton-Raphson fluxes \bar{f}_i are

$$\begin{aligned}
\bar{f}_1 &= \bar{\rho} \bar{u} \\
\bar{f}_2 &= \bar{\rho} \bar{u}^2 + (\gamma - 1) \left(\bar{\rho} \left[\bar{e} - \frac{\bar{u}^2}{2} \right] \right) - \frac{1}{\text{Re}} \bar{\tau} \\
\bar{f}_3 &= \bar{\rho} \bar{u} \bar{e} - \frac{\gamma}{\text{RePr}} \bar{w} + (\gamma - 1) \bar{\rho} \bar{u} \left(\bar{e} - \frac{\bar{u}^2}{2} \right) - \frac{1}{\text{Re}} \bar{\tau} \bar{u} \\
\bar{f}_4 &= \nu \bar{u} \\
\bar{f}_5 &= \mu \left(\bar{e} - \frac{\bar{u}^2}{2} \right)
\end{aligned}$$

4.2 Implementation Notes

4.2.1 Enforcing boundary conditions

Since our boundary conditions are enforced on the linearized problem, we can only enforce the Rankine-Hugoniot normal shock conditions on u indirectly by enforcing boundary conditions on Δu .

If we examine the fluxes \bar{f}_i that depend on our previous solution, we can see that \bar{f}_1, \bar{f}_4 , and \bar{f}_5 only depend on ρ , u , and e , whose boundary values are determined by the normal shock conditions. Setting $u(0) = u_a$ equal to the Mach number Ma and $\rho(0) = \rho_a = 1$, we can determine ρ_b, u_b, e_a and e_b .

We set our initial guesses for ρ , u , and e such that

$$\begin{aligned}\rho(0) &= \rho_a, & \rho(1) &= \rho_b \\ u(0) &= u_a, & u(1) &= u_b \\ e(0) &= e_a, & e(1) &= e_b\end{aligned}$$

and use those values to determine the values of the fluxes \bar{f}_1 , \bar{f}_4 , and \bar{f}_5 at the boundaries. Then, by setting the fluxes of our Newton-Raphson update Δu at the boundaries equal to zero, we enforce that each accumulated solution $u + \Delta u$ satisfies our normal shock conditions.

4.2.2 Line Search

Our early implementations of the solver used an unweighted Newton-Raphson step, such that our update looked like

$$u := u + \Delta u$$

Since intermediate Newton-Raphson solutions showed significant undershoots and overshoots, our solution variables often displayed non-physical values, such as negative density or internal energy. In these cases, Newton-Raphson would often fail to converge. To avoid this, we used a weighted Newton-Raphson step,

$$u := u + \alpha \Delta u$$

where we allowed α to vary depending on u and Δu .

```
Set  $\alpha = 1$ .
Set constraintFlag = 0.
do while constraintFlag = 0
    Set  $\alpha := \alpha/2$ 
    if  $\rho$  and thermal energy  $\geq 0$ 
        constraintFlag = 1
    end of if loop
end of while loop
```

Figure 14: Simple line search algorithm for determining Newton-Raphson step size α .

To select α , we used a simple line search algorithm, summarized in Fig. 14. Whenever the sum of Δu and the previous solution u would take on non-physical values (our constraint), we would divide the Newton-Raphson step by two. If the new Newton-Raphson step still causes the solution to take on non-physical values, we divide again by two, repeating until $u + \alpha \Delta u$ is physical.

4.2.3 Adaptivity

As described above, we use the “poor-man’s” hp -adaptivity scheme described in Fig. 4 that refines in h until the smallest element width is smaller than the shock width, after which it refines in p . The shock width for our stationary shock solution is given by

$$\delta_s = \frac{1}{Re(M-1)^2}$$

In practice, we found

$$\delta_s = \frac{8}{Re(M-1)^2}$$

to be a more effective measure of the shock width.

4.3 Numerical Results

We note that, since Burgers is derived from Navier-Stokes, the numerical sensitivity of the boundary conditions for Burgers also affects solutions for Navier-Stokes.

4.3.1 Low Reynolds numbers

For the calculations in this section, we’ve used the weighted, mesh-independent inner product mentioned earlier

$$(v, \delta v) = \int_{x_{k-1}}^{x_k} (v' \delta v' + v \delta v) \alpha(x) dx$$

We again use our inner Newton-Raphson refinement scheme described in Fig. 5. Fig. 4.3.1 and Fig. 4.3.1 are plots of the solution for $Re = 10^2$ and $Ma = 2$.

Note that our adaptivity scheme uses a single mesh for all solution variables; hence, refinement is guided by the combined error over all solution components.

In the error plots in Fig. 17 and Fig. 18, we note similarities to the error plots for Burgers’ equation; both exhibit similar jumps of $\|\triangle u\|_E$ and the nonlinear residual at refinements, and for both, the error decreases monotonically as a function of degrees of freedom.

4.3.2 Results for higher Reynolds numbers

For higher Reynolds numbers, we use a mesh-dependent weighted inner product which improves the conditioning of the stiffness matrix when there are large gradients in the solution.

$$(v, \delta v) = \int_{x_{k-1}}^{x_k} (h_k v' \delta v' + v \delta v) \alpha(x) dx$$

where h_k is the k th element size.

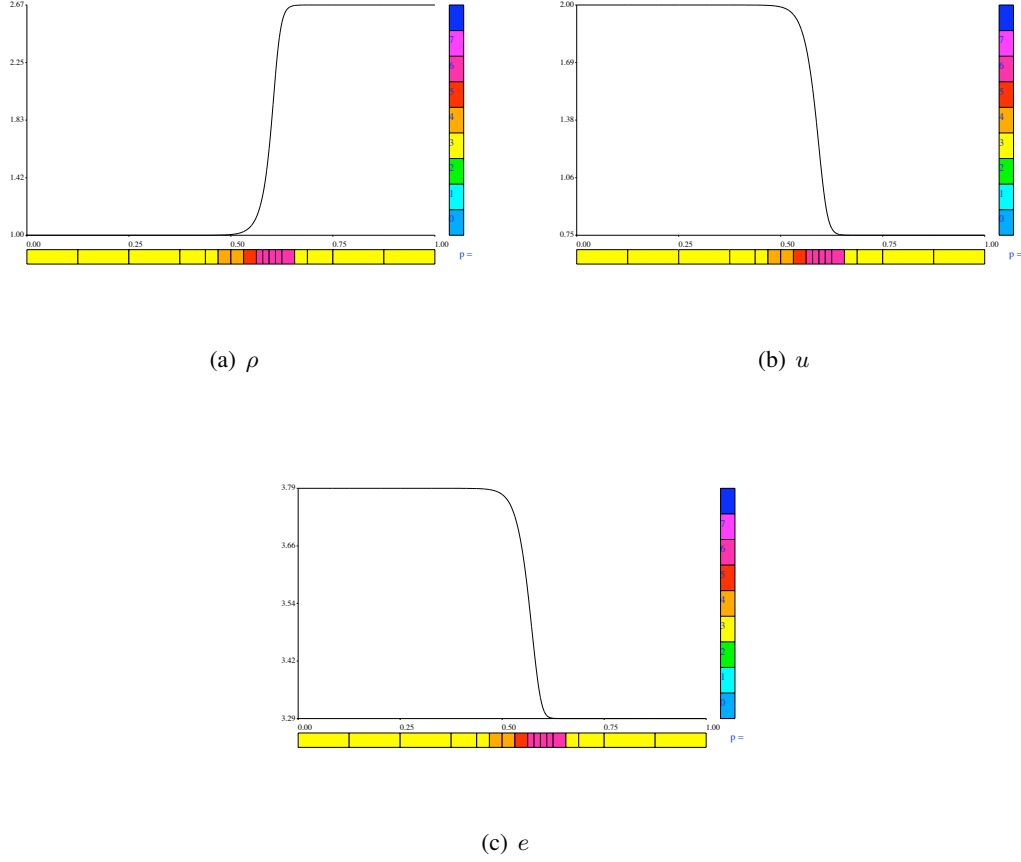


Figure 15: ρ , u , and e for $\text{Re} = 10^2$ and $\text{Ma} = 2$ after 10 refinements with an initial mesh of 8 quadratic elements, with $\|\triangle u\|_E = 6.349 \times 10^{-11}$ and nonlinear residual 7.9776×10^{-10} .

Fig. 19 shows the zoomed-out velocity u after a certain number of refinements. Qualitatively, the other solution variables look similar, and at this length scale, these solutions give little information. Zooming in near the shock for a finer resolution of the solutions shows that the shock is in fact a smooth function, and resembles qualitatively the solutions obtained for lower Reynolds numbers.

Due to the sensitivity of the solution to boundary conditions, after the mesh is refined to the point of being able to resolve the shock width, the shock location tends to shift around. As a consequence, $\|\triangle u\|_E$ begins to oscillate between refinements instead of decreasing monotonically. The result is similar to what we observed with Burgers' equation—convergence to a particular solution doesn't make sense in light of a numerically non-unique solution.

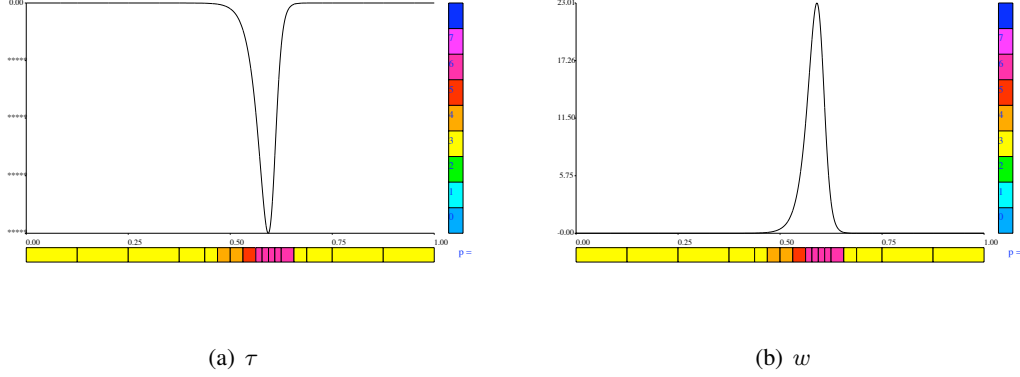


Figure 16: Viscous stress τ and heat flux w for $\text{Re} = 10^2$ and $\text{Ma} = 2$ after 10 refinements.

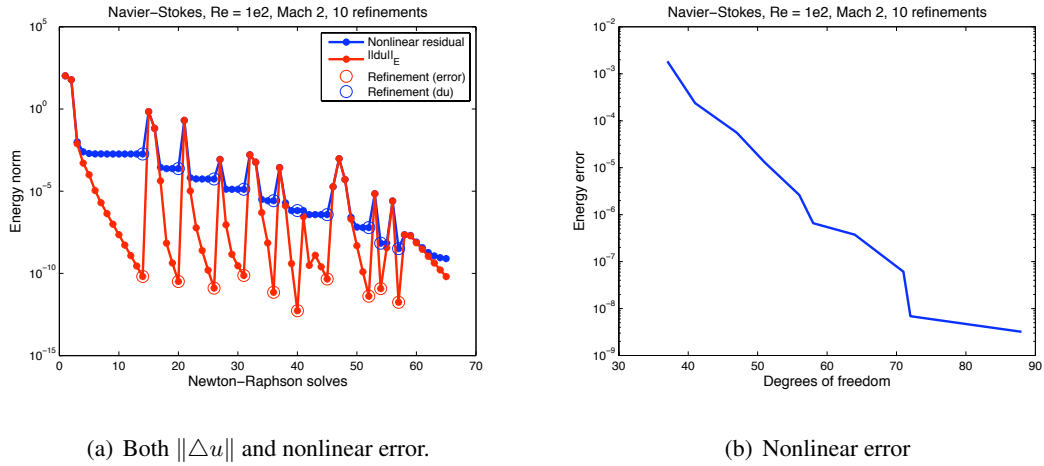
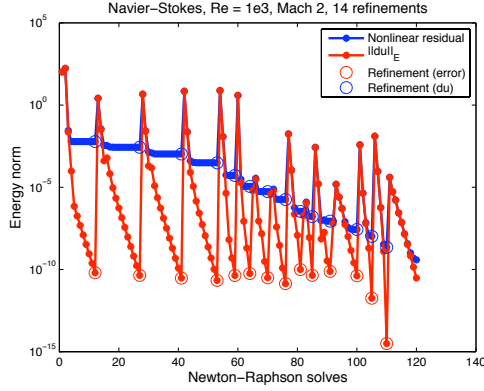


Figure 17: Navier-Stokes error plots for $\text{Re} = 10^2$ and $\text{Ma} = 2$, with $\|\Delta u\| = 6.34923 \times 10^{-11}$ and nonlinear residual 7.977×10^{-10} .

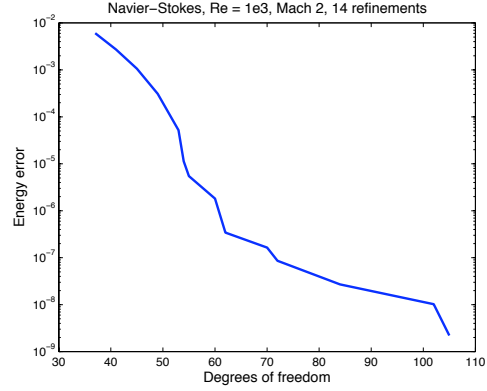
5 Conclusions and Further work

We've formulated a methodology for applying DPG to nonlinear problems, including a strategy for doing hp -refinements with Newton-Raphson iterates. We've also introduced measures of convergence for the nonlinear problem ($\|\Delta u\|_E$ and the nonlinear residual).

For modest shock widths, numerical experiments have shown monotonic decrease of the nonlinear residual as the number of degrees of freedom increase. While we haven't been able to drive our nonlinear residual to machine zero for very small shock widths (due to sensitivity of the Burgers' and Navier-Stokes equations to perturbations in the boundary conditions), we believe that the problems are simply artifacts of the 1D test problems we've chosen.



(a) Both $\|\Delta u\|$ and nonlinear error.



(b) Nonlinear error

Figure 18: Navier-Stokes error plots for $\text{Re} = 10^3$ and $\text{Ma} = 2$, with $\|\Delta u\| = 3.02496 \times 10^{-11}$ and nonlinear residual 3.8336×10^{-10} .

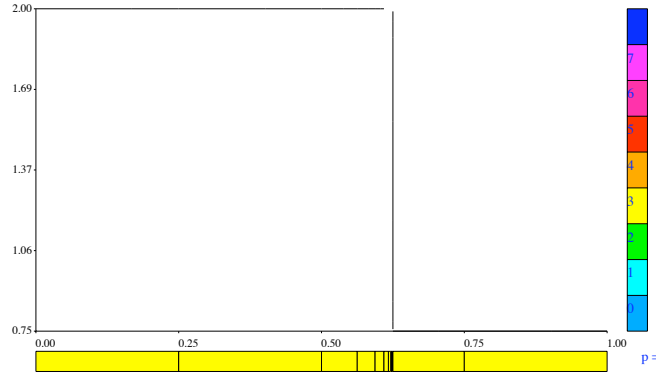


Figure 19: Zoomed out u for $\text{Re} = 10^{10}$ and $\text{Ma} = 2$.

We hope to study alternative strategies for doing hp -refinements in context of a Newton-Raphson linearization. Theoretically, we hope to be able to prove the well-posedness of our nonlinear variational problems. Future work also includes applying these methodologies to 2D shock problems in fluid dynamics, by first studying DPG's behavior on reduced problems (Burgers' equation, incompressible Euler equations, the Stokes equation), then by implementing DPG for the isentropic Navier-Stokes, from which we hope to move on to the full 2D compressible Navier-Stokes equations.

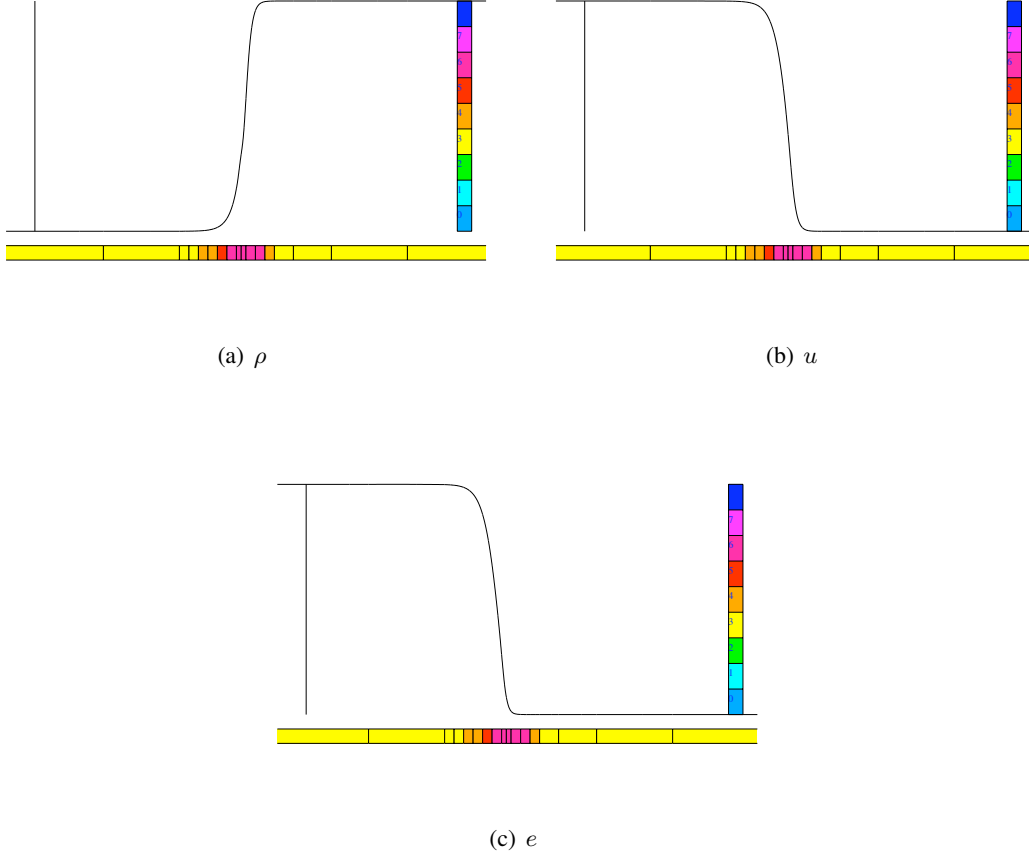


Figure 20: Zoomed in (by a factor of 10^9) ρ , u , and e for $\text{Re} = 10^{10}$ and $\text{Ma} = 2$.

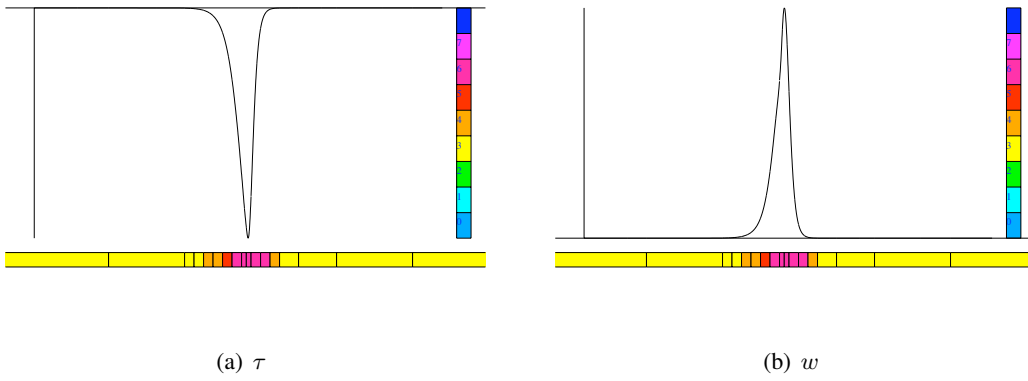


Figure 21: Zoomed in viscous stress τ and heat flux w for $\text{Re} = 10^{10}$ and $\text{Ma} = 2$.

References

- [1] J.D. Anderson. *Modern Compressible Flow With Historical Perspective*. McGraw–Hill, Boston, 3rd edition, 2004.
- [2] I. Babuška. Error-bounds for finite element method. *Numer. Math*, 16, 1970/1971.
- [3] Garrett E. Barter. *Shock Capturing with PDE-Based Artificial Viscosity for an Adaptive, Higher-Order Discontinuous Galerkin Finite Element Method*. PhD thesis in Aeronautics and Astronautics, Massachusetts Institute of Technology, 2008.
- [4] C.L. Bottasso, S. Micheletti, and R. Sacco. The discontinuous Petrov-Galerkin method for elliptic problems. *Comput. Methods Appl. Mech. Engrg.*, 191:3391–3409, 2002.
- [5] C.L. Bottasso, S. Micheletti, and R. Sacco. A multiscale formulation of the discontinuous Petrov-Galerkin method for advective-diffusive problems. *Comput. Methods Appl. Mech. Engrg.*, 194:2819–2838, 2005.
- [6] A. N. Brooks and T. J. R. Hughes. Streamline upwind/petrov-galerkin formulations for convection dominated flows with particular emphasis on the incompressible navier-stokes equations. *Computer Methods in Applied Mechanics and Engineering*, 32(1-3):199–259, 1982.
- [7] P. Causin and R. Sacco. A discontinuous Petrov-Galerkin method with Lagrangian multipliers for second order elliptic problems. *SIAM J. Numer. Anal.*, 43, 2005.
- [8] P. Causin, R. Sacco, and C.L. Bottasso. Flux-upwind stabilization of the discontinuous Petrov-Galerkin formulation with Lagrange multipliers for advection-diffusion problems. *M2AN Math. Model. Numer. Anal.*, 39:1087–1114, 2005.
- [9] Juan Cheng and Chi-Wang Shu. High order schemes for cfd: a review. Technical report, Brown University, 2009.
- [10] T.J. Chung. *Computational Fluid Dynamics*. Cambridge University Press, 1st edition edition, 2002.
- [11] B. Cockburn and C. W. Shu. The runge kutta discontinuous galerkin method for conservation laws v multidimensional systems. *Journal of Comp. Phys.*, 141(2):199–224, 1998.
- [12] J. D. Cole. On a quasi-linear parabolic equation occurring in aerodynamics. *Quarterly of Appl. Math.*, 9(3):225–236, 1951.
- [13] L. Demkowicz and J. Gopalakrishnan. A class of discontinuous Petrov-Galerkin methods. Part I: The transport equation. *Comput. Methods Appl. Mech. Engrg.*, 2009. accepted, see also ICES Report 2009-12.

- [14] L. Demkowicz and J. Gopalakrishnan. A class of discontinuous Petrov-Galerkin methods. Part II: Optimal test functions. Technical Report 16, ICES, 2009. Numer. Meth. Part. D. E., in review.
- [15] L. Demkowicz, J. Gopalakrishnan, and A. Niemi. A class of discontinuous Petrov-Galerkin methods. Part III: Adaptivity. Technical Report 1, ICES, 2010.
- [16] L. Demkowicz, J.T. Oden, and R. Rachowicz. A new finite element method for solving compressible Navier-Stokes equations based on an operator splitting method and hp adaptivity. *Comput. Methods Appl. Mech. Engrg.*, 84:275–326, 1990.
- [17] A. Harten, B. Engquist, S. Osher, and S. Chakravarthy. Uniformly high-order accurate non-oscillatory schemes. *SIAM Journal on Numerical Analysis*, 24(1):279–309, 1987.
- [18] Eberhard Hopf. The partial differential equation $u_t + uu_x = \mu u_{xx}$. *Comm. Pure and Appl. Math.*, 3:201–230, 1950.
- [19] X.D. Liu, S. Osher, and T. Chan. Weighted essentially nonoscillatory schemes. *Journal of Comp. Phys.*, 115:200–212, 1994.
- [20] J.M. Melenk. *hp-Finite Element Methods for Singular Perturbations*. Springer, Berlin, 2002.
- [21] J.T. Oden and L.F. Demkowicz. *Applied Functional Analysis for Science and Engineering*. Chapman & Hall/CRC Press, Boca Raton, 2010. Second edition.
- [22] W.H. Reed and T.R. Hill. Triangular mesh methods for the neutron transport equation. Technical Report LA-UR-73-479, Los Alamos Scientific Laboratory, 1973.
- [23] C. Schwab and M. Suri. The p and hp versions of the finite element method for problems with boundary layers. *Math. Comput.*, 65(216):1403–1429, 1996.
- [24] C. W. Shu. Essentially non-oscillatory and weighted essentially non-oscillatory schemes for hyperbolic conservation laws. Lecture notes, Brown University.